Biophys. Struct. Mech. 7, 65–95 (1980)

Biophysics of Structure and Mechanism

Electrondensity Profile Determination of Bacterial Photosynthetic Membranes*

N. Hodapp and W. Kreutz

Institut für Biophysik und Strahlenbiologie der Universität Freiburg im Breisgau, Albertstraße 23, D-7800 Feiburg i. Br., Federal Republic of Germany

Abstract. X-ray diffraction experiments with stacks of wet, oriented bacterial thylacoids were performed. The main result is the determination of the electrondensity profile, which is the projection of the electrondensity of the membrane stack onto the stacking axis. Our evaluation procedure takes into account statistical deviations of the quasi-crystalline arrangement of membranes in the stack, differences between the electrondensities in the interthylacoid space and the thylacoid lumen, the statistical distribution of the stack lengths and differences between the mean electrondensity of the stacks and the surrounding medium. Electronmicroscopical determination of parameters describing the statistical lattice deviations in freeze fractured specimens, prepared in the same way as for X-ray diffraction, showed that the influence of membrane undulations can be neglected. They also provided information concerning the validity of the model assumption of lattice deviations of the second kind [27]. The procedure for evaluation which we describe also yielded an absolute calibrated electrondensity scale for the final structure. This profile enabled to be determined the distribution of the membrane components with respect to their position along the stacking axis to be estimated.

Key words: Photosynthetic bacteria – Electronmicroscopy – X-Ray diffraction

Introduction

Although the photosynthetic apparatus of procaryotic cells differs considerably from that of eucaryotic cells with respect both to morphological and metabolic aspects, the principal mechanism of the transfer of light energy is the same. As the photosystem of procaryotes shows increased stability because of its simpler structure and at the same time possesses a high adaptability to changed external

* Dedicated to Prof. W. Menke on the occasion of his 70th birthday

0340-1057/80/0007/0065/$ 06.20

conditions, they serve as a good object for the study of the photosynthetic primary processes and their structural basis. For structural investigations of the bacterial photosynthetic membrane, electronmicroscopic techniques and X-ray diffraction analysis have been used. The evaluation of freeze etch electron-micrographs has allowed the determination of the frequency and size of particles, which seem to cover the luminal as well as the cytoplasmic surface of the thylacoids [1–4]. Further, the freeze fracture technique also allows the determination of the frequency and size of the intramembranous particles [4–6]. Unfortunately, with deep freeze techniques, morphological changes may occur, caused by the freezing procedure or anti freezing compounds [7, 8], so that especially quantitative evaluations of such micrographs should be made with a certain reserve. By contrast, artefacts and denaturation can be largely excluded in X-ray diffraction techniques. Up to now few X-ray small angle studies with bacterial thylacoids have been carried out. Ueki et al. [9] evaluated the equatorial scattering intensity of ordered lamellar bacterial thylacoid systems resulting in an hexagonal plane membrane lattice. Pape et al. [10] determined, by means of a method introduced by Weick [11], the electrondensity profile of spherical bacterial thylacoid membrane vesicles. The profile is the projection of the membrane electrondensity onto an axis perpendicular to the membrane surface.

The determination of the electrondensity profile of stacked thylacoids, as carried out with chloroplasts of higher plants by Kreutz [12–14], and with algal chloroplasts by Sadler et al. [15] have not yet been carried out with bacterial photosynthetic membranes. In a recent paper a new method was introduced [16] for the determination of the electrondensity profile of lamellar systems, taking into account the experimentally unavoidable distortions of the membrane lattices in the X-ray specimens in a more comprehensive way than other authors do. This treatment takes into consideration not only the separation statistics between the thylacoid membranes but also the electrondensity in the intermembranous space from the mean electron density of the scattering regions. Furthermore, it also considers membrane deformations which can be described by statistical appearance of membrane undulations.

The aim of our studies was the determination of the elctrondensity profile of thylacoid stacks of the photosynthetic bacterium Rhodopseudomonas viridis. Further, a comparison between parameters describing the statistical distortions of the membrane lattices, obtained by X-ray diffraction and electronmicroscopy, could be made.

Materials and Methods

Growth Conditions

Rhodopseudomonas viridis were grown in a culture medium for athiorhodaceae [17] under light intensities of 1,300–1,500 Lux. They were harvested after the end of the logarithmic growth. The temperature in the light cabinet was about 29° C.

Thylacoid Preparations

The cells were washed several times in 0.05 M Tris-HCl buffer pH 7.2. The washed pellet was used for X-ray diffraction experiments with whole cells. Thylacoids were isolated by grinding cells with aluminium oxide in a mortar for about 3 min [18]. After resuspending in Tris buffer, whole cells and large cell fragments were removed by a centrifugation at 15,000 g. The supernatant was centrifuged at 100,000 g for 60 min. The pellet of this centrifugation will be referred to as crude thylacoid preparation.

Purification of the Crude Thylacoid Preparation

For further purification, especially to remove ribosomal contamination, the resuspended crude thylacoid preparation was layered on to a 30%–45% sucrose gradient in Tris buffer. The strongly pigmented band with a density of 1.16–1.17 g/cm^3 was collected and washed two times in Tris buffer to remove sucrose. The washed pellet will be referred to as purified thylacoid preparation.

Determination of the Protein and Phospholipid Content

The protein content of the density-gradient-purified thylacoids was determined according to the method of Lowry et al. [19]. The content of the phospholipids was determined by a procedure of Bartlett [20]. One share of the membrane suspension was dried in a desiccator over phosphorpentoxide for four weeks. Protein and phospholipid content were related to the dry weight.

Recording of X-ray Diffraction Patterns

For the recording of the X-ray diffraction patterns the wet pellets of the different preparations were placed into a special humidity chamber [21] which was equipped with special lead blades for the present investigation (Fig. 1). A droplet of the wet pellet was mounted between the blades. The shape of the blades, the surface tension of the specimen and the water release to the surrounding atmosphere leads to the transformation of the droplet into a platelet shape. This shape favours the alignement of the thylacoid membranes parallel to the surfaces of the platelet. The X-rays pass the humidity chamber through Na-acetate or polyester windows of about 10 μm thickness. The relative humidity in the chamber is stabilized by distilled water or special salt solutions which are poured into the lower part of the chamber. The humidity chamber was built for the use in Kiessig cameras; with special adjusting equipment it could also be used in Kratky cameras. For general survey, recording was carried out in a Kiessig camera [22] or in a Rigaku mirror camera. The cross section of the primary beam was 0.5 mm respectively 100 μm × 100 μm. The specimen to film

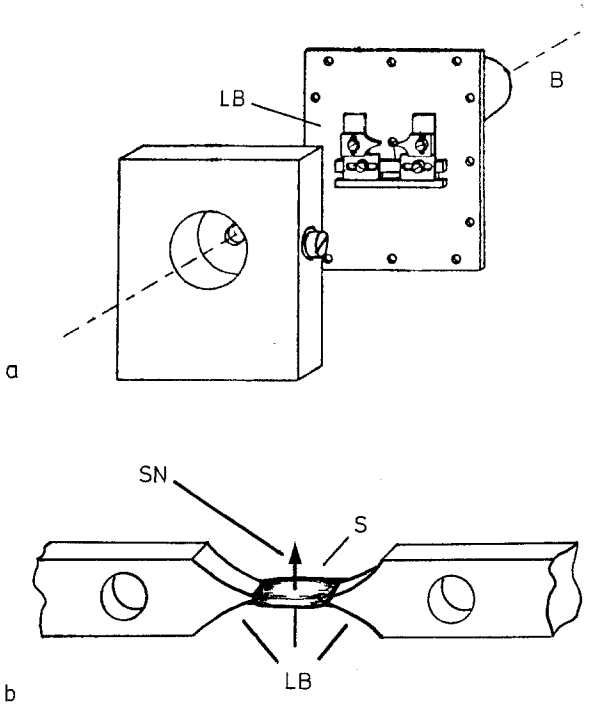

Fig. 1. a Humidity chamber for the thylacoid specimen during X-ray exposure (Müller-Klieser, Kreutz [21]). The humidity chamber is vacuum-tight and filled with a few cm^3 of water or salt solution to guarantee a constant atmospherical humidity. The specimen is mounted between lead blades (*LB*). The dotted line shows the course of the X-ray beam (*B*). **b** Lead blades with mounted specimen. A drop of the wet centrifugation sediment (*S*) is placed between the blades (*LB*). Surface tension and loss of water favour a platelet-like shaping of the specimen. Membrane stacks in the specimen orient with their stacking axes around a preferred direction (*SN*)

distance was 50 cm respectively 20 cm. The diffraction pattern was recorded on Kodak Kodirex films. X-ray diffraction for the determination of the electron-density profiles was carried out with Kratky cameras [23]. The height of the primary beam was 100 μm, the lateral extension was limited by additional diaphragms to 150 μm. Registration was performed with a Siemens-Braun position sensitive high pressure proportional counter [24]. The specimen to counter distance was 20–25 cm. The diffraction intensity was measured in the direction of the preferred orientation of the membrane stack normals. For the recording of the isotropic background scattering the detector was rotated by 30° referred to the preferential scattering direction of the oriented stacks.

The difference between the intensity in the preferred direction and the isotropic background scattering was smoothed to eliminate statistical noise. Smoothing was carried out by means of a method given by Bevington [25] which folds the measured intensity with a triangle function of variable basis length. A comparison between a spline-method smoothing [26] and the triangle smoothing showed no significant differences, so that the Bevington method was preferred as it required less computing time than the spline program.

As an X-ray source a rotating anode generator Rigaku Rotaflex RU 200 V with a copper target was used. The operating characteristics were 45 KV tube voltage and 200 mA tube current. All X-ray investigations were performed at room temperature.

Determination of the Electrondensity Profile from the Experimental Scattering Intensity

For the evaluation of the X-ray diffraction patterns, as presented in this paper, the method given in [16] was applied as briefly outlined in the following. For more details the original paper should be consulted. The procedure describes the scattering specimen as an ensemble of coherent scattering membrane stacks. Their model scattering intensity is fitted to the experimental intensity by a least square fit program. The model scattering intensity is calculated via the Q-function [27].

The following assumptions regarding the properties of the scattering specimen are essential for the applicability of the model:

(1a) The specimen consists of stacks built up by single membranes with an image mirror-image sequence. The lateral extension of the membranes is large compared with its expansion in the direction of the stack axis.

(1b) The axes of the membranes stacks possess a distribution of their orientation. This distribution may be described by a statistical distribution function around a preferential alignment.

(1c) The number n_s of the image mirror-image membrane pairs in one stack is fluctuating. Its mean value is $\langle n_s \rangle$. The following expression should hold

$$\sigma(n_s) \ll \langle n_s \rangle \ll N_{\mathbf{r}} ,$$

were $\sigma(n_s)$ is the standard deviation of the n_s and $N_{\mathbf{r}}$ the number of stacks with the stacking axis aligned parallel to $\mathbf{r}$.

(1d) The distance between the membranes of one vesicle fluctuated according to a distribution function H_1. The distance between two neighboured membranes of different vesicles fluctuate according to a distribution function H_2. The lattice distortions should be of the second kind [27, 28], that means that distance fluctuations do not refer to fixed lattice points but are independent of each other.

(1e) Luminal and cytoplasmic electrondensity may have different values, that means the electrondensity projection of the thylacoid lumen can have another level than that of the electrondensity projection of the interthylacoid space. Both levels may also be different from the mean electrondensity of the stack.

(1f) All membranes may have slight bulges and recesses. These will be referred to as undulations.

(1g) The scattering intensity of the specimen is caused by the incoherent superposition of the individual stack intensities.

For the description of a stack the electrondensity profile of a half period in the stacking direction is used. It will be referred to as half period profile. The

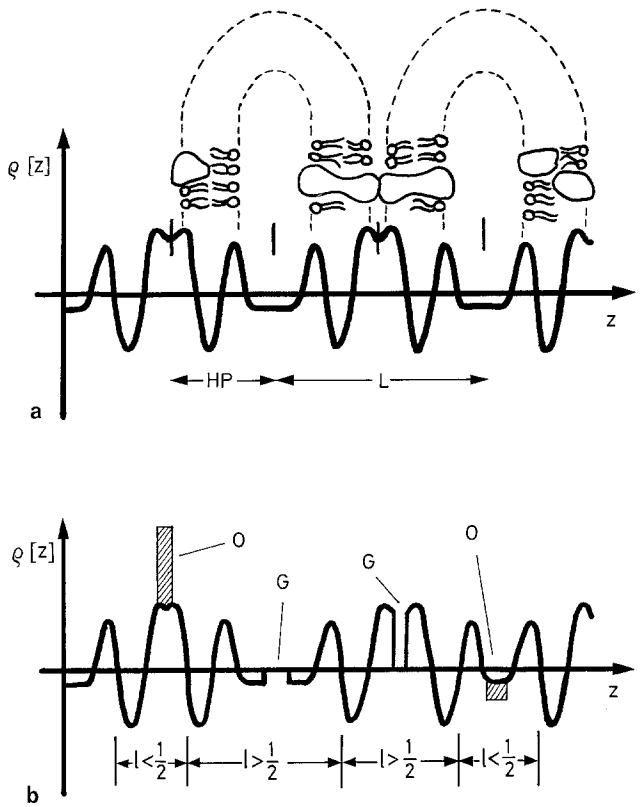

Fig. 2. a Electrondensity profile of a fictitious membrane stack with five half periods (*HP*) without statistical distortions. Two half periods form the profile of a vesicle as well as a part of the surrounding medium. The vesicle share is schematically demonstrated. The period length (*L*) has an extension of two half periods. It is equated with the experimentally determined value of the Bragg distance. **b** Electrondensity layer profile with statistically fluctuating distances between the centers of the half periods. The hatched overlappings (*O*) and the gaps (*G*) are corrected by subtraction respectively by addition of appropriate box functions

half period profile comprises the electrondensity of a single membrane and also one half of the intermembranous space at both sides of the membranes.

The alternating arrangement of image and mirror-image of such half-period profiles forms the profile of the stack, possessing the properties described in assumption *(1a)*. Distance fluctuations between individual membranes are considered by Gauss-shaped distance statistics [see assumption *(1d)*]. Overlappings and holes between statistically distributed half-periods, which are due to the fact that the electrondensity in the intermembranous spaces can differ from the mean value of the surrounding medium, are corrected by addition or subtraction of adequate box functions. As an example in Fig. 2a and b the electrondensity profile of a statistically undisturbed and a disturbed fictitious membrane stack is demonstrated. The convolution square of a statistically disturbed stack with different electrondensities in the interspaces can be

described as a sum of convolution terms of the building-block-functions and the correction step function. The statement contained in assumption *(1g)* means that the scattering intensity is an incoherent superposition of individual, coherent scattering stacks. As averaging and Fourier transformation may be permuted, a mean Q-function of the following shape is given:

$$Q = \langle Q_{s,\phi} \rangle_s \,. \tag{1}$$

$Q_{s,\phi}$ is the Q-function of an individual stack characterized by the index s with a special orientation of the stacking axis characterized by ϕ. If $Q_{s,\phi}$ is described by means of the building-block, we obtain with an appropriate manner of summation, as shown in [16]:

$$\begin{aligned}
\langle Q_s, \phi \rangle_s = & \sum_{j=0}^{n_s \max} \langle n_s - j \rangle_s \cdot 2 \, \tilde{\tilde{\varrho}}_{\bar{M}} * (H_1 \overset{j}{\frown} H_2) \\
& + \sum_{j=0}^{n_s \max} \langle n_s - j \rangle_s \cdot (\varrho_{\bar{M}} * \varrho_{\bar{M}} * H_1) * (H_1 \overset{j}{\frown} H_2) \\
& + \sum_{j=0}^{n_s \max} \langle n_s - j - 1 \rangle_s \cdot (\varrho_M * \varrho_M * H_2) * (H_1 \overset{j}{\frown} H_2) \\
& + \sum_{j=0}^{n_s \max} \langle n_s - j \rangle_s \cdot 2 \, (\varrho_{\bar{M}} * zpI) * (H_1 \overset{j}{\frown} H_2) \\
& + \sum_{j=0}^{n_s \max} \langle n_s - j - 1 \rangle \cdot 2 \, (\varrho_{\mathrm{M}} * zpI * H_2) * (H_1 \overset{j}{\frown} H_2) \\
& + \sum_{j=0}^{n_s \max} \langle n_s - j - 1 \rangle_s \cdot 2 \, (\varrho_M * zpE) * (H_1 \overset{j}{\frown} H_2) \\
& + \sum_{j=0}^{n_s \max} \langle n_s - j - 1 \rangle_s \cdot 2 \, (\varrho_{\bar{M}} * zpE * H_1) * (H_1 \overset{j}{\frown} H_2) \\
& + \sum_{j=0}^{n_s \max} \langle n_s - j - 2 \rangle_s \cdot (zpE * zpE * H_1) * (H_1 \overset{j}{\frown} H_2) \\
& + \sum_{j=0}^{n_s \max} \langle n_s - j - 1 \rangle_s \cdot (zpI * zpI * H_2) * (H_1 \overset{j}{\frown} H_2) \\
& + \sum_{j=0}^{n_s \max} \langle n_s - j - 1 \rangle_s \cdot 2 \, (zpI * zpE) * (H_1 \overset{j}{\frown} H_2) \\
& + \langle n_s \rangle_s \, zqI + \langle n_s - 1 \rangle_s \, zqE \,.
\end{aligned} \tag{2}$$

The range in which the Q-function is described is confined to the positive values of the coordinate axis parallel to the stacking axis.

The following definitions are used:

ϱ_M = Half period profile

$\varrho_{\bar{M}}$ = Mirror image of the half period profile

$*, \overset{j}{\frown}$ = Convolution operations

$\overset{2}{\sim}$ = Convolution square

H_1, H_2 = Gauss-shaped statistic functions for the description of the distance fluctuations between the half-period centers

n_s = Number of the double membranes (vesicles) in a stack with index s

$$zpI = \begin{cases} -h_I \phi\left(\dfrac{z - d/2}{\sigma_1}\right) & \text{for } z < d/2\,, \\ h_I\left[1 - \phi\left(\dfrac{z - d/2}{\sigma_1}\right)\right] & \text{for } z > d/2\,, \end{cases}$$

where h_I = deviation of the electrondensity of the vesicle lumen with respect to the mean electrondensity of the stack, ϕ = Gaussian error function, d = extension of the half period in the direction of the stacking axis, σ_1 = standard deviation of the Gaussian statistic H_1 of the vesicle lumen extension.

zpE = Equivalent function for the contact area of different vesicles. h_I has to be replaced by h_E = deviation of the electrondensity in the vesicle interspace from the mean electrondensity of the stack. In the same way σ_1 has to be replaced by σ_2 which is the standard deviation of the statistic function H_2.

zpI and zpE are the sum of the correction functions, weighted according to their frequences.

$$zqI = \frac{2\,h_I^2\,\sigma_1}{\sqrt{2\pi}} e^{-\frac{z^2}{2\sigma_1^2}} - 2\,h_I^2 \cdot z \cdot \phi\left(\frac{-z}{\sigma_1}\right)$$

$$zqE = \frac{2\,h_E^2\,\sigma_2}{\sqrt{2\pi}} e^{-\frac{z^2}{2\sigma_2^2}} - 2\,h_E^2 \cdot z \cdot \phi\left(\frac{-z}{\sigma_2}\right)$$

The above formula of the mean Q-function is only valid for an ensemble of stacks with plane membranes and parallel alignment of the stack normals. This simple model allows the reduction of the evaluation to a one-dimensional problem. The consideration of membrane undulations requires the transition to a threedimensional description of the stack electrondensity. The parameters used in [16] to describe the undulation behaviour of the membranes will be treated more detailed, because the same kind of parameters were used for the description of the statistical behaviour observed in electronmicroscopy. In [16] a

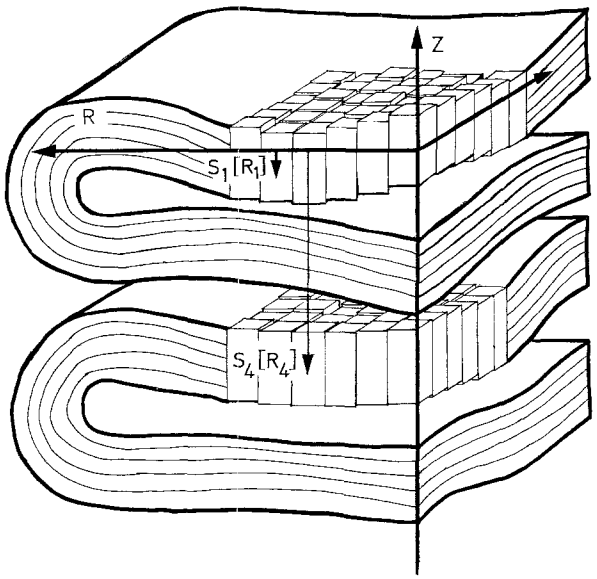

Fig. 3. Description of membrane undulations by partitioning the membrane into infinitesimal columns. The undulations will be described by displacing the centers of infinitesimal membrane columns in z-direction. As a measure of displacement the standard deviation of the displacement distances as a function of the lateral distance R for all columns with the same R between them is used. For example the standard deviation of all $S_1(R_1)$ is a measure for the correlation decrease within the membranes themselves, the standard deviation of all $S_4(R_4)$ is a measure for the correlation decrease as a function of the lateral shifting of two membranes with a single period distance

function $s\ (R, \theta)$ is introduced for each membrane, describing the displacement of the half period centers in the direction of the stacking axis as a function of the lateral coordinates R and θ. The membrane is thus built up by means of the function $s\ (R, \theta)$ and infinitesimally thin columns, whose z-dependence on the electrondensity is given by $\varrho(z)$ (Fig. 3). By means of this presentation it is possible to describe the influence of the membrane undulation of the undisturbed Q-function by a correction function for the contributions to the mean Q-function as listed in equation (2). The dependence of the mean Q-function on lateral coordinates is no longer constant. The larger the distance R from the origin of the coordinate system becomes, the broader becomes the distribution function, giving the position of the convolution terms of individual infinitesimal columns, by which the convolution square of the considered membrane density is composed. A description of the dependence of the mean Q-function on the lateral angle is unnecessary due to averaging the convolution terms of many stacks. To correct the undulation influence, the following specified function:

$$H^{u}_{k,j}(z) = \frac{1}{\sqrt{2\pi}\, A_{k,j} \cdot R}\, e^{-\frac{z^2}{2 A^2_{k,j} R^2}}$$

has to be folded with each addend in Eq. (2).

This function is a Gaussian distribution with a standard deviation linearly dependent on R. The increase of the R-dependence on the one hand depends on the kind of convolution term given in Eq. (2), characterized by the index k, and on the other hand on the summation index j of the considered convolution term. Concretely this means: the dependence of the standard deviation of the function $H^u_{k,j}$ on the indices k and j is a measure for the correlation decrease of the considered stack elements with respect to the lateral displacement of one of the involved elements. The influence of the undulations on the scattering intensity is expressed in a lateral broading of the diffraction orders, caused by an apparent decrease of the lateral coherent scattering area. Recording along a path through the centers of the sickle-shaped diffraction orders therefore comprehends the scattering contributions of a decreasing number of stacks. This is taken into account by the integral:

$$I_{\exp}(b_z) \sim \int_0^{\pi} h(\alpha) \sin(\alpha) I^u_{ST}(b_z, \alpha)\, d\alpha ,$$

where b_z is the coordinate of the preferred direction of the stack normals, $h(\alpha)$ the distribution of the frequency of stack normals with regard to the preferred direction and $I^u_{ST}(b_z, \alpha)$ is the intensity of all stacks with an angle α between the stacking axis b_z. A minimal number of scanning points of the model intensity in the direction of the sickle centers is then fitted to an adequate number of scanning points of the experimental intensity by a least squares fit procedure. In order to reduce the number of model parameters, we tried to determine the parameters for the description of the statistical membrane behaviour by evaluation of the electronmicrographs. We therefore prepared thylacoids under the same conditions as for X-ray diffraction experiments and freeze fractured them after a stay of 24 h in the humidity chamber. 31 electronmicrographs were evaluated. At a total magnification of 1 : 2,000,000 the curve of the membrane centers was scanned and stored with the help of a digitizer. The scanning distance was 1 nm in units of the true membrane size. The following statistical parameters were calculated by a computer program:

(2a) The Self-Correlation of the Membranes. The standard deviation $\sigma(R)$ of the distance in z-direction between all scanning points of one membrane ($j = 0$) with lateral distance R averaged over all membranes of one stack was calculated. The course of the R-dependence will be compared with the linear formulation for the standard deviation. Moreover, the ascent of the correlation decrease has to be determined.

(2b) The Undulation Correlation Between Different Membranes. The R-dependence of the standard deviation σ of the distance in z-direction between the scanning points of different membranes was determined by j as a further parameter. The assumption regarding the correlation decrease with increasing j will be examined.

(2c) Distance Statistics. The evaluation of the standard deviation for the distance of membrane points with $R = 0$ as a function of j should show whether the assumption of lattice distortions of the second kind holds or not.

The results obtained by such evaluations showed, as will be dealt with later, that the influence of membrane undulations on the scattering intensity can be neglected in the case of the specimen in question. In the following evaluations of the scattering intensities the membrane model was reduced to the specimen properties stated in *(1a–e)* and *(1g)*. Another phenomenon of the observed intensities led to a further modification of the membrane model. As already described, although the scattering intensity along the direction of the sickle centers was corrected by subtraction of the isotropic part of the scattering intensity, the difference curve showed a considerable amount of continuous scattering also below the peaks of higher diffraction orders. This high oriented background scattering could not be described within the facilities given in *(1a–g)*. Since, however, an arbitrary consideration of this oriented background scattering, either by manual subtraction or by fitting a suitable analytical function, has a strong influence on the solution profile, we attempted to consider this oriented background as a part of the model. For this purpose we had to abandon the assumption in [16] of very large vesicle stacks. This procedure was developed from the following considerations:

The standard deviation of the distance statistics as well as the extension of the stacks in the direction of the stacking axis influence the extension of the diffraction orders in meridional direction.

Hosemann ad Bagchi [27] and Vainshtein [28] gave equations which state the relation.

$$IW^h(m, \sigma_s) = \sqrt{(IW_s^h)^2 + \left(\frac{1}{m\,L}\right)^2}\,.$$

$IW^h(m,\sigma_s)$ is the integral width of the diffraction order with index h, m is the number of periods L in a stack and

$$IW_s^h = 1 - \exp\frac{(-2\pi\sigma_s^2\,h^2)}{2\,L}$$

is the contribution of the lattice factor to the width of the diffraction orders, caused by the standard deviation σ_s of the distance statistics of one period.

Therefore σ_s and m can be estimated with the help of two IW^h values with different hours. The estimation led to an average stack extension of about 4–5 periods. As such stacks are relatively short and because a distribution of the stack lengths has to be taken into account ("finite model") there certainly must be stacks whose scattering intensity of the mean electrondensity cannot be neglected. Therefore, the Fourier series, which describes the half period profiles in the "infinite" model, was extended by the contribution of the 0th coefficient. This shift was taken into account for all addends listed in equation [2]. As a reasonable formulation for the distribution of the stack lengths an exponential distribution was taken,

$$e^{-\frac{a}{a_0}}$$

were a_0 is the mean value of the stack lengths. The mean value of the stack lengths was estimated by the experimental intensity as given above. The dependence of the model intensity on the structure parameters admits no straight-forward evaluation of these parameters. Therefore, the parameters were determined by a least-squares-fit procedure. We used a procedure developed by Marquardt [29]. Prior to the fit the experimental intensity was scanned. The scanning interval is given by the Shannon theorem [30]. The scanning interval must be smaller than the reciprocal extension of the Q-function in the z-direction. A criterion for the quality of the fit is the so-called ϕ-value were $\phi = \sum_p (I_{\text{exp}} - I_{\text{mod}})^2$ and p is the number of scanning points of the Shannon-scanned intensity. As the computing duration of the computer program strongly depends upon the quality of the approximation of the starting values, it is advisable to find criteria for the choice of the starting values. Statistical parameters and stack extension may be estimated as described. The moduli of the starting values for the Fourier coefficients are approximately evaluated by the height or the area of the diffraction orders. The number of the necessary Fourier coefficients is restricted by the number of diffraction orders. In the case of undisturbed lattices with narrow diffraction orders all sets of Fourier coefficients, arising through randomly changing the signs, are also solutions of the problem. For a set of n Fourier coefficients there are 2^n solutions. In the case of a disturbed lattice the number of solutions can be limited since the product of lattice function (square of the modulus of the Fourier transformed distribution function of the lattice distances) and the structure factor (square of the modulus of the Fourier transformed period profile) gives additional information about the structure factor due to the broadening of the lattice function peaks. If one starts a fit for each possible sign combination of the Fourier coefficients (phases), the sign combination, whose Fourier series represents the solution should then yield the lowest ϕ-value. Half period profiles differing only by a common sign for all Fourier coefficients, i.e., profiles which become identical by reflecting at the abscissa, do not differ with respect to the quality of the fit. Both, image and mirror-image, must therefore be discussed as possible solutions. Experimental intensities with large noise or models which inadequately describe the specimen properties may lead to several different profiles with comparable fit quality. This means, that several different profiles fit the experimental intensity with similar ϕ-values. In this case either model or measurement must be improved. If, after the fit only few phase sets remain, additional critera, which can be obtained from other experiments, may be sufficient to exclude further phase sets.

Electronmicroscopic Studies

Electronmicroscopic studies were made primarily to control the purity of the crude thylacoid preparation, and secondly to determine the statistical parameters. For the puritiy control thin suspensions of the crude thylacoid preparation were contrasted with 2% phosphotungstic acid. Special care was taken for the detection of serious impurities, caused by whole or incompletely opened cells. In

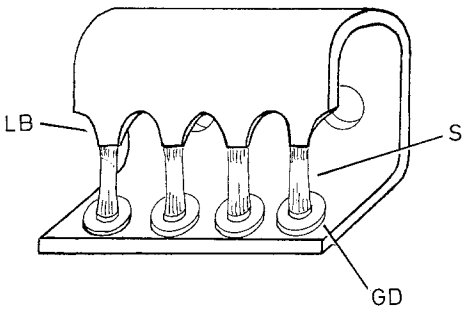

Fig. 4. Sample carrier for the production of freeze fracture specimens under similar conditions as during X-ray exposure. The specimen (*S*) were stretched between gold disks (*GD*) and lead blades (*LB*) and the sample carrier was kept for 24 h in an X-ray humidity chamber

order to determine statistical parameters, similar specimens, as used in X-ray experiments, were prepared. Viscous drops of the thylacoid sediment were placed between gold disks and lead blades and were stretched subsequently (Fig. 4). An arrangement of four samples was put into a humidity chamber for 24 h. The lead blades were then removed and the samples freeze fractured.

Results

Determination of the Water Content

X-ray diffraction specimens as well as those prepared under similar conditions for electronmicroscopic determination of the statistical parameters show a considerable loss of water during the first day, although they were kept in the humidity chamber above destilled water. The fresh specimens contained about 3.00 ± 0.3 g water per gram of dry weight above phosphorpentoxide. Within 24 h the water share decreased to about 0.75 ± 0.25 g/g. This ratio of water content to specimen dry weight of about 1:1 remained constant for at least several days. Measurements with a humidity sensitive capacitor showed that the relative humidity in the chamber was about $94 \pm 1\%$. These results agree with data given in [31].

Protein and Lipid Content

The determination of the protein and phospholipid content yielded a relative protein share of 50% and a phospholipid share of 30% relative to the dry weight. These results are in accordance with data given by Drews [32].

Electronmicroscopic Results

Freeze fracture replicae of thylacoid specimen kept in a humidity chamber for 24 h, were not of the quality of those obtained with freshly fractured specimens.

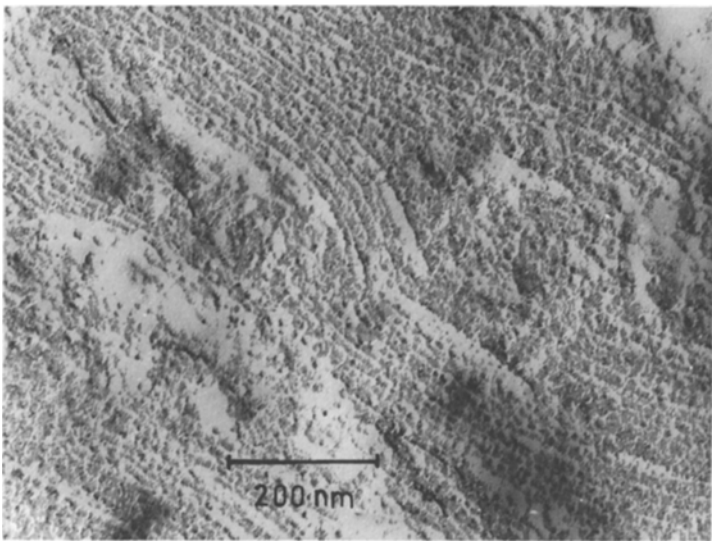

Fig. 5. Freeze fracture electronmicrographs of a crude thylacoid preparation. The specimens were freeze fractured after a period of 24 h in the humidity chamber. The water content of the specimens decreased during this period in the humidity chamber to 1/5 of the original value. Large cross fractures of lamellar arrays can be clearly seen, which alternate with regions, where the membranes are aggregated to small groups only

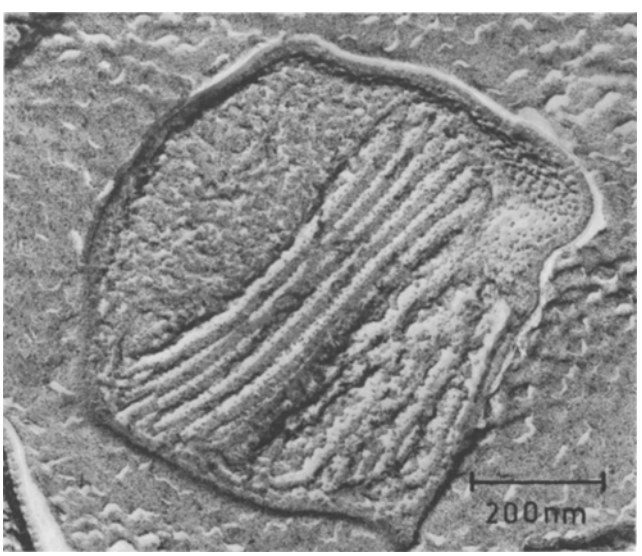

Fig. 6. Freeze fracture electronmicrograph of whole bacteria without stay in the humidity chamber. The interthylacoid membrane distance is smaller than the intrathylacoid distance. It is more distinctly marked than with isolated thylacoids. The period length is larger than in Fig. 5 because the specimen did not suffer a humidity loss

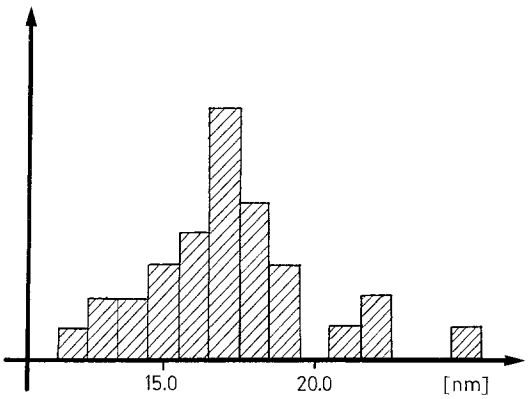

Fig. 7. Frequency distribution of the period lengths. The periods were evaluated by means of 31 electronmicrographs of stacks similar to those shown in Fig. 5

This may be ascribed to the altered composition caused by the loss of water. In spite of this, many areas showed fractures of lamellar arrangements. A representative micrograph of such areas is shown in Fig. 5. In contrast Fig. 6 shows a freeze fracture micrograph of whole bacteria in the wet state. The evaluation of 31 micrographs showed strong fluctuations of the mean period length between different stacks. Figure 7 shows the distribution of the period length for the evaluated micrographs. It must be mentioned, that the model in [16] does not take into account fluctuations of the period lengths of individual stacks. If this phenomenon is taken into consideration there are two effects on the model intensity. The first: a small but usually negligible modification in the intermembranous space-correction-function; the second: the standard deviation of the statistics functions H_1 and H_2 must be interpreted in another way (the distance statistics now include the distance fluctuations of all stacks and not only those of one individual stack). Table 1 presents the results of the statistic parameter determination. Figure 8 shows the R-dependence on the correlation diminuition of four membrane pairings within the first two periods, evaluated for one of the 31 stacks. The A-values in Table 1 were calculated by means of the ascent of such curves. The standard deviations of the distance statistics take into account the undulation influence on the Q-function at $R = 0$. A comparison between the electronmicroscopic A-values and model calculations in [16], which yielded 0.1 as lower limit of A for the influcence of undulations on the diffraction pattern, show, that nearly all A-values lie below this value. Therefore, membrane undulations do not affect the X-ray diffraction pattern of such stacks. A systematic increase of the A-values with increasing distance between the correlated membranes was not observed. The evaluation of the distance statistics parameters showed that the propagation of the lattice distortions is not correctly described by the model of lattice distortions of the second kind. But as the broadening of the distance statistics with increasing membrane distance is more appropriately described by lattice distortions of the second kind than by other assumptions the procedure was not modified with respect to this point.

Table 1. Electronmicroscopically determined statistical parameters of 31 stacks

No.[a]	D_1[b] [nm]	D_2[c] [nm]	σ_1[d] [nm]	σ_2[e] [nm]	P[f] [nm]	σ_p[g] [nm]	σ_{th}[h] [nm]	A_1[i]	A_2[j]	A_3[k]
1	11.1	13.6	2.7	2.7	24.6	3.4	3.8	0.1	0.00	0.01
2	10.3	10.3	0.9	1.5	20.6	1.5	1.7	0.06	0.03	0.03
3	11.3	11.3	2.4	1.8	21.7	3.1	3.0	0.08	0.03	0.03
4	9.4	12.5	4.0	3.6	21.6	3.3	5.4	0.09	0.09	0.00
5	9.0	9.3	1.1	1.8	18.0	2.0	2.1	0.05	0.02	0.01
6	8.2	10.6	1.1	2.7	18.8	3.2	2.9	0.07	0.03	0.00
7	8.8	9.0	1.4	1.4	17.6	1.8	2.0	0.08	0.05	0.02
8	6.4	9.5	1.1	2.2	15.9	2.2	2.5	0.06	0.01	0.00
9	6.6	8.6	1.6	2.7	15.2	3.3	3.1	0.05	0.00	0.1
10	6.6	7.1	1.5	1.2	13.5	1.6	1.9	0.05	0.01	0.02
11	6.4	6.4	0.9	1.1	12.9	1.4	1.4	0.06	0.03	0.01
12	7.1	10.9	1.1	1.5	17.4	2.0	1.9	0.04	0.00	0.01
13	8.3	9.2	1.5	1.6	17.3	2.2	2.2	0.09	0.05	0.05
14	8.4	8.8	1.6	1.5	17.3	1.8	2.2	0.08	0.03	0.04
15	7.8	9.4	1.8	2.4	17.3	3.2	3.0	0.01	0.04	0.04
16	5.4	6.7	1.0	1.1	12.1	1.1	1.5	0.05	0.02	0.01
17	6.5	6.5	0.9	1.8	13.3	1.0	2.0	0.03	0.00	0.01
18	6.5	8.1	1.8	1.7	14.3	2.1	2.5	0.06	0.02	0.00
19	7.6	9.7	2.2	2.5	17.5	2.9	3.3	0.08	0.00	0.01
20	7.3	8.2	1.3	1.9	15.5	2.3	2.3	0.09	0.03	0.02
21	8.1	10.2	1.4	1.6	18.5	2.1	2.1	0.07	0.03	0.02
22	7.9	8.9	1.5	2.1	16.7	2.2	2.6	0.07	0.00	0.03
23	8.5	9.1	1.4	2.0	17.4	2.7	2.4	0.11	0.06	0.03
24	8.9	10.3	1.2	2.3	19.2	2.1	2.6	0.13	0.09	0.07
25	7.3	8.5	1.9	2.7	15.7	2.6	3.3	0.08	0.02	0.00
26	6.2	9.1	1.2	1.7	15.6	2.1	2.1	0.06	0.01	0.00
27	8.1	9.1	1.5	1.7	17.2	2.1	2.3	0.06	0.02	0.01
28	6.3	8.7	0.9	1.6	14.8	1.5	1.8	0.04	0.01	0.0
29	6.4	8.3	0.8	0.9	15.1	1.1	1.2	0.03	0.00	0.00
30	7.4	9.7	1.0	1.5	17.4	1.8	1.8	0.06	0.00	0.03
31	8.6	9.6	1.3	1.3	18.3	1.6	1.8	0.06	0.01	0.02
MV[l]	7.83	9.26	1.48	1.87	17.0	2.16	2.41	0.066	0.02	0.02

[a] No. = Number of the stack
[b] D_1 = Mean value of the distances between the centers of adjacent membranes belonging to neighboured thylacoids
[c] D_2 = Mean value of the distances between the centers of membranes belonging to the same vesicle
[d] σ_1 = Standard devitation of D_1
[e] σ_2 = Standard devitation of D_2
[f] P = Mean period length in the stack
[g] σ_p = Standard devitation of P
[h] σ_{th} = Theoretical value for σ_p, in the case of lattice distortions of the second kind $\sigma_{th} = \sqrt{\sigma_1^2 + \sigma_2^2}$
[i] A_1 = Undulation parameter for the self-correlation of the membranes as described in „Materials and Methods"
[j] A_2 = Undulation parameter for the correlation between adjacent membranes of neighboured thylacoids
[k] A_3 = Undulation parameter for the correlation between membranes belonging to the same thylacoid
[l] MV = Mean values for the above listed columns

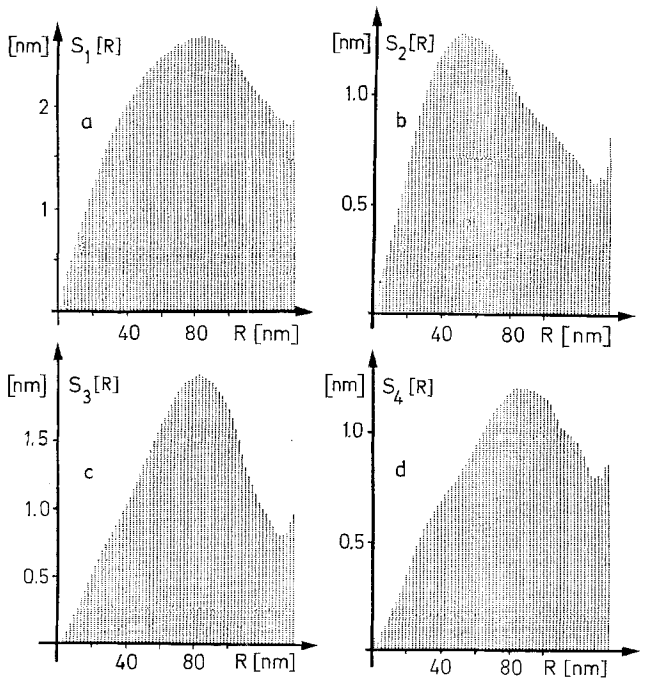

Fig. 8a–d. R-dependence of the correlation decrease for undulation function pairs for one distinct stack of the evaluated freeze fracture electronmicrographs. **a** Shows the *R*-dependence of the standard deviation of position distances in *z*-direction averaged over all self-paired membranes. **b** and **c** Show the *R*-dependence for the neighbouring membranes with only interthylacoid space respectively intrathylacoid space between them. **d** Shows the correlation dependence for membrane pairings with one period between them. The four figures show that the assumption in [16] postulating a linear *R*-dependence holds fairly well for the relevant inner part of the function

X-Ray Diffraction Results

X-ray diffraction patterns, recorded on films, of crude thylacoid preparations as well as such of whole bacteria show preferred orientation (Fig. 9) which was achieved by mounting the specimen between lead blades. The diffraction patterns shown represent a series of about 40 similar recordings. Always the 2nd, 3rd, 4th, and 5th order of a series with sickle-shaped diffraction spots, which belong to Bragg distances of about 17.5 ± 1.5 nm, are observed. The aperture angle of the sickles is 17.5 ± 5° to both sides of the preferential orientation. The exposure time for such patterns was about 24 h to achieve a good density on the film. Changes of the diffraction intensity before the humidity equilibrium is reached, can therefore not be resolved. This could only be done when using a position sensitive proportional counter (PSP-Counter). The minimal registration time required by the signal-noise-ratio was about 2.8 h ~ 10,000 s.

Figure 10 shows time series of spectra with 2.8 measuring time each. Figure 10a gives the dependence of the scattering intensity measured at a crude thylacoid specimen in an intact humidity chamber. After 18–27 h the intensity

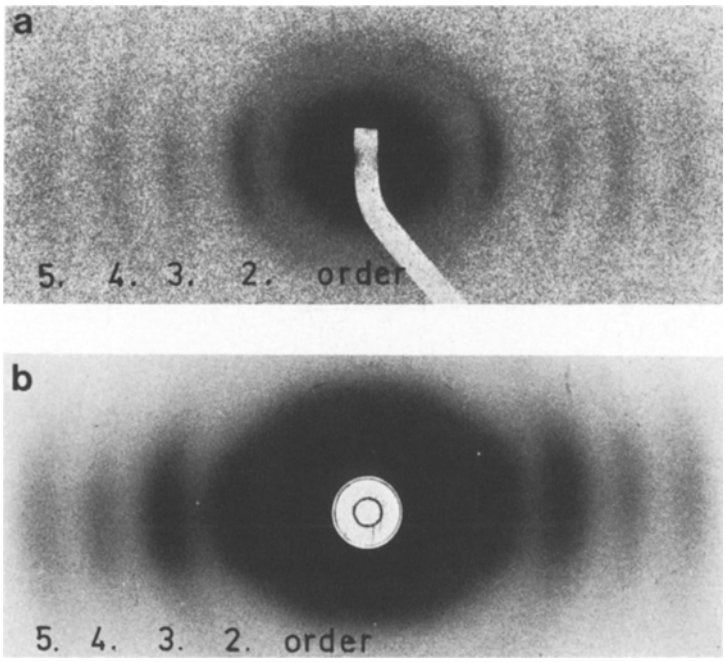

Fig. 9a and b. X-ray diffraction intensities recorded on film. **a** Shows the diffraction intensity of a crude thylacoid preparation, recorded in a Rigaku mirror camera. The specimen-to-film-distance was 20 cm, the registration time was 24 h. The diffraction orders have a Bragg-distance of 17.3 nm. **b** Shows the diffraction intensity of whole bacteria recorded in a Kiessig camera. The specimen-to-film-distance was 50 cm, the registration time was 24 h. Both records show an orientation of the diffraction order series. The Bragg-period is 17.5 nm

stabilizes and remains constant for at least two days. Figure 10b shows the time dependence of the scattering intensity where the humidity equilibrium could not be attained due to leakage of the humidity chamber. In this case, there is a continuous decrease of the spacing accompanied by a broadening of the lower and disappearance of the higher diffraction orders. Since the time for reaching the equilibrium of hydration agrees with the time required to stabilize the diffraction intensity, it is clear that the changes in the diffraction intensity accompany the loss of water from the specimen. The intensity curves, as shwon in Fig. 11 still contain the isotropic part of the diffraction intensity. Unfortunately, the evaluation of diffraction intensities, before reaching the humidity equilibrium, is not possible, for the following reasons:

(3a) The changes in the spectra are too fast during that period. As a minimum of about 3 h exposure time is necessary, each spectrum contains the superposition of several states.

(3b) In order to carry out a reasonable evaluation, the isotropic background must be known. It is, however, not measurable simultaneously due to equipment conditions. Because of the rapid intensity changes, differences between stacking intensity and background intensity are too inaccurate.

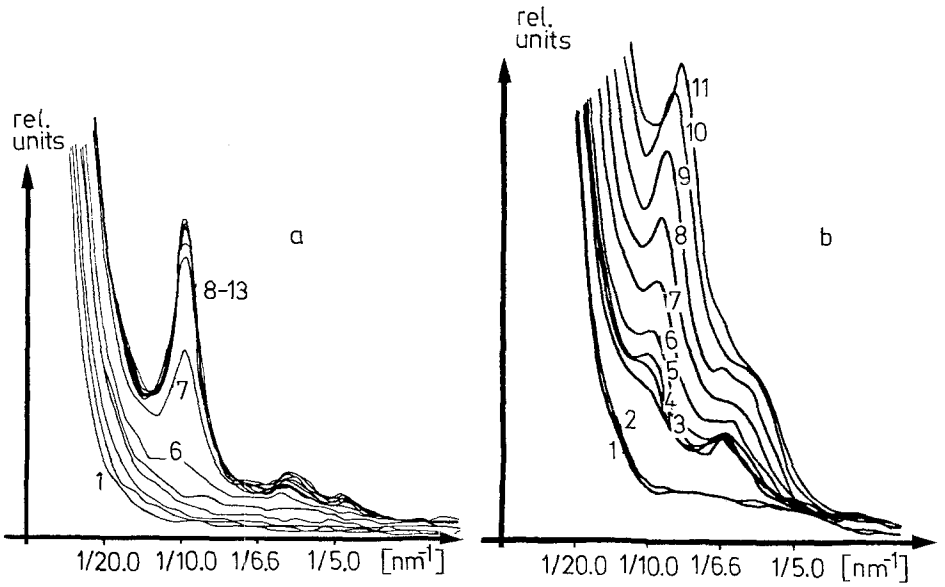

Fig. 10a and b. Time dependence of the diffraction intensity. **a** Shows the smoothed diffraction intensities of a crude membrane preparation without background correction, recorded in 2.8 h intervals according to the sequence numbers with a PSP-counter. After 24–27 h the diffraction intensity remains constant. Comparative measurements showed, that this runs parallel to reaching the humidity equilibrium in the specimen. During the recording time of the intensity **b** the humidity equilibrium could not be reached due to leakage in the chamber window. Therefore, the diffraction intensity also changed beyond 27 h after placing the sample into the chamber. The beginning of the recording intervals lasting 2.8 h for the various spectra was as follows: 1.9 h for 1, 5.8 h for 2, 16.9 h for 3, 21.8 h for 4, 24.5 h for 5 after filling the humidity chamber and for the subsequent spectra 2.8 h each later on

(3c) Moreover, difference curves between stack intensity and isotropic background as a rule have a worse signal-noise-ratio; thus, a longer exposure time would be necessary. This is not possible due to the diffculties mentioned in *(3a)*.

For this reason electrondensity calculations were only carried out with diffraction intensities measured after reaching the humidity equilibrium, that means, at least 18–27 h after placing the specimen into the humidity chamber. The 3 h registration intervals were retained to detect possible intensity changes during the stable phase. Spectra which showed no differences were summed up to improve the signal-noise-ratio. After 6–9 h measurement in the preferred direction of the stack axes, the PSP-counter was rotated about 30° to measure the isotropic background scattering. These measurements also showed no significant changes during the humidity equilibrium phase. About 3–6 spectra were summed up and isotropic scattering intensity of equal exposure time was subtracted. The difference curve was smoothed, Lorentz-corrected and Shannon-scanned. In most cases a scan with 10 points per diffraction-order-distance was chosen. This scan admits a maximum length of 10 periods for the Q-function. Because of the lattice distortions this interval suffices also for

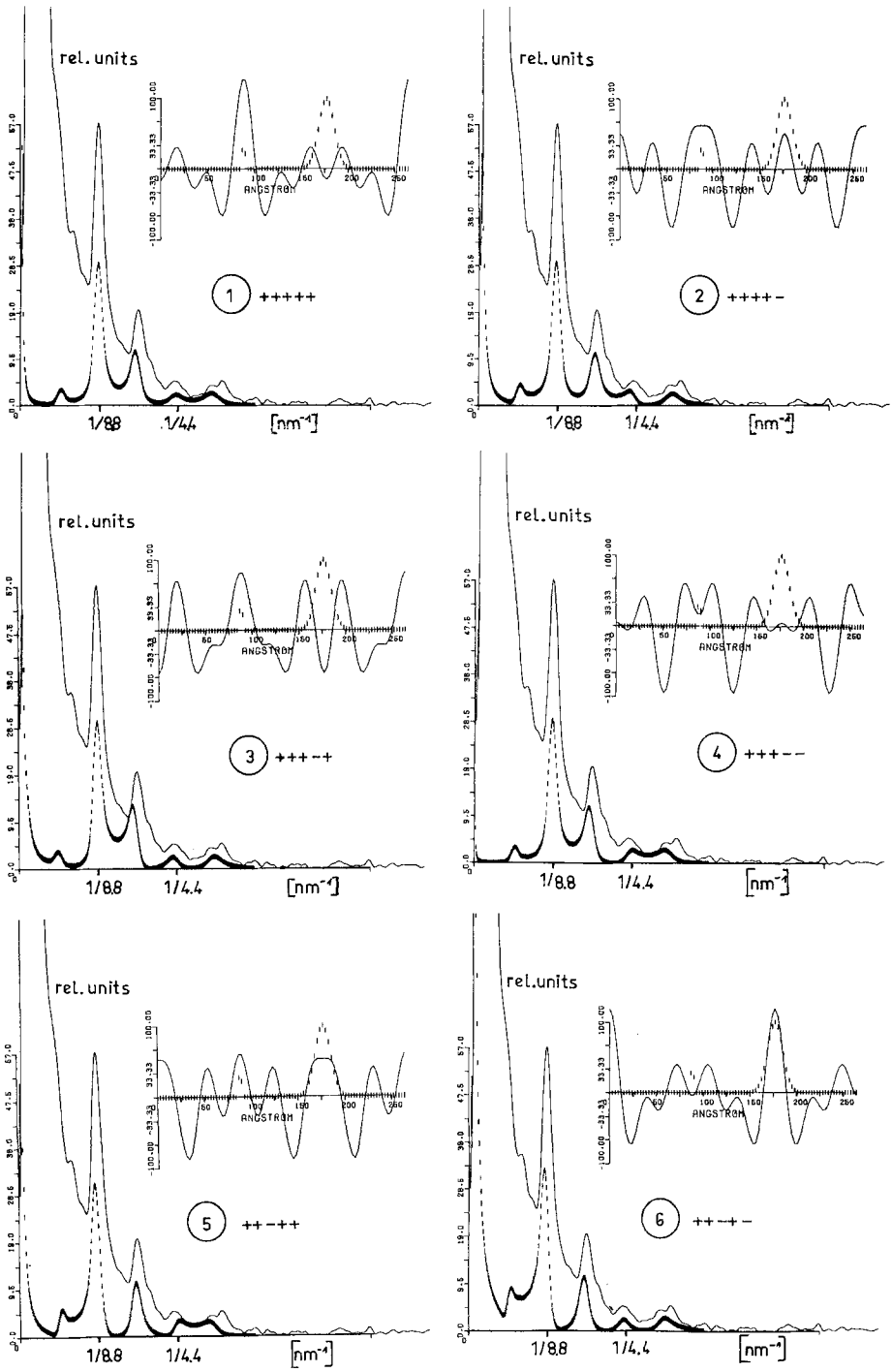

Fig. 11. (Legend see page 86)

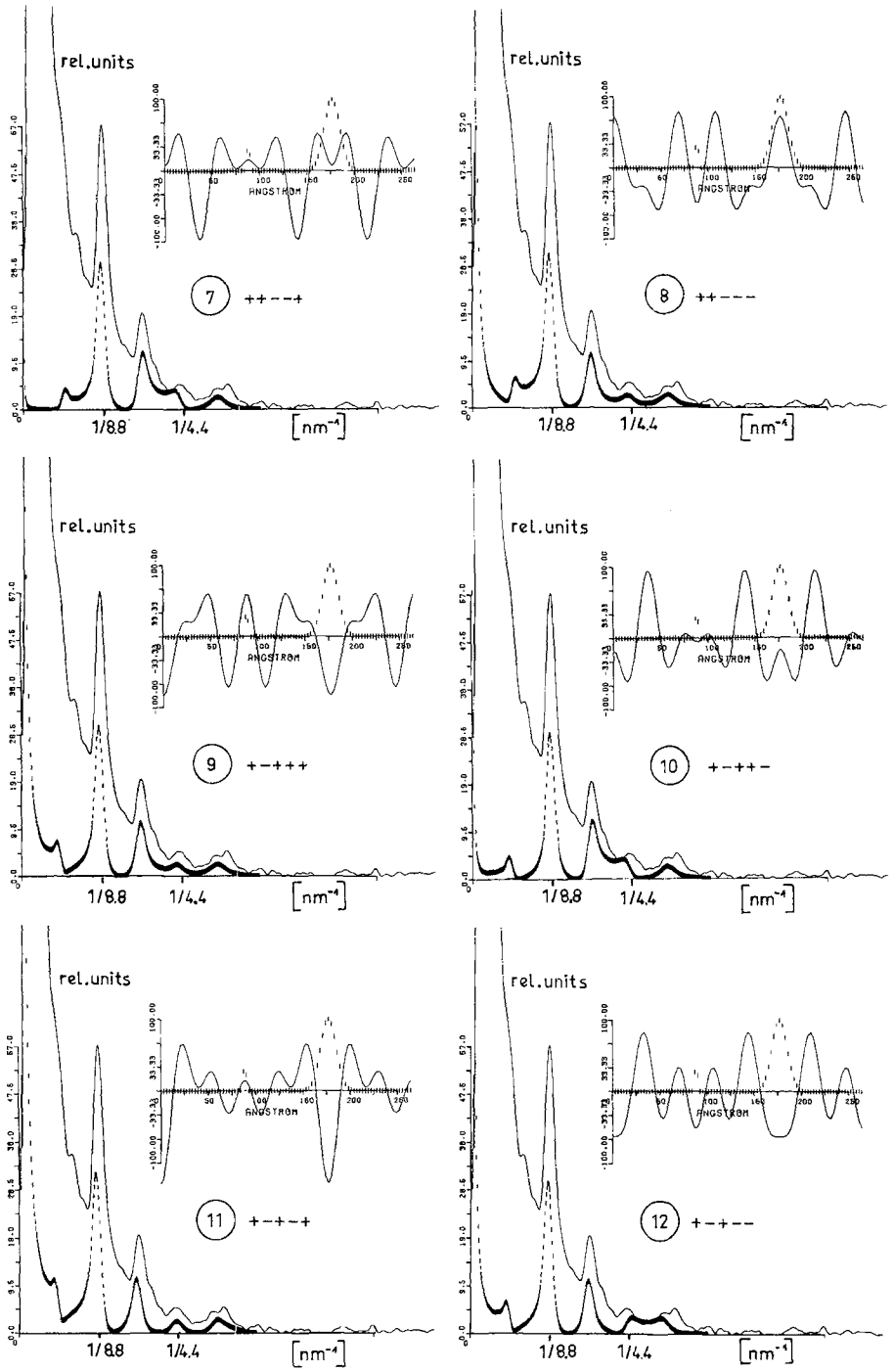

Fig. 11. (Legend see page 86)

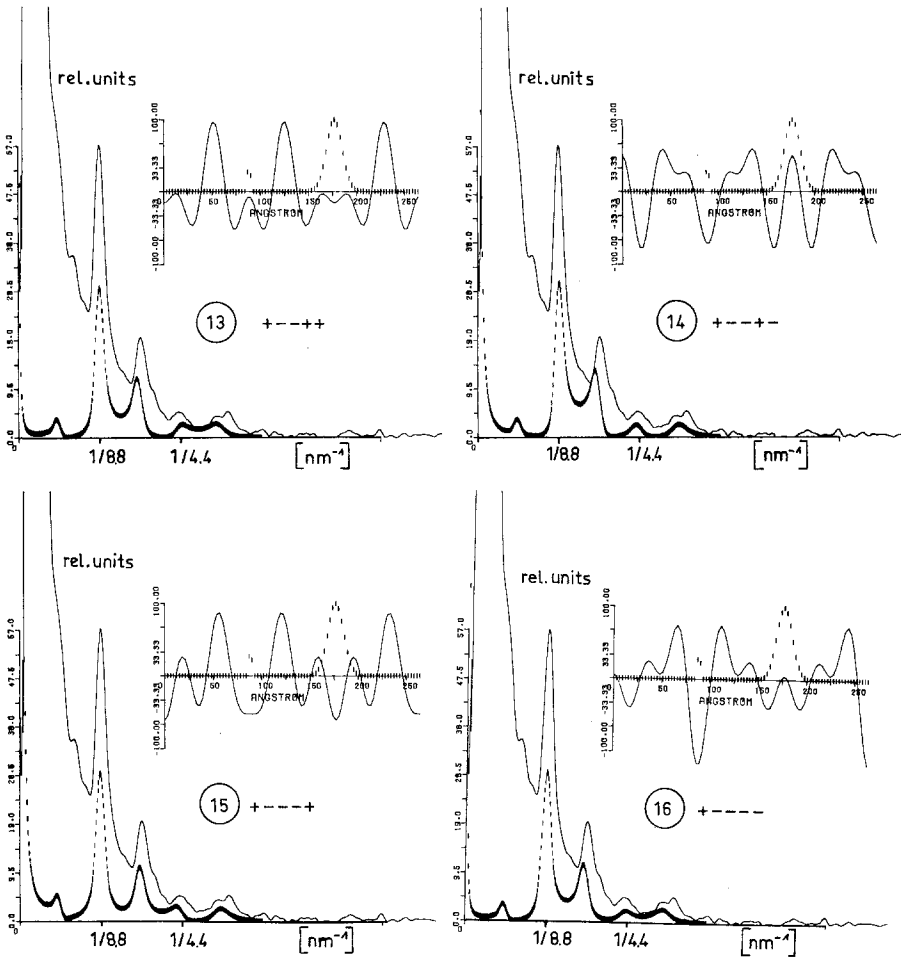

Fig. 11. Electrondensity profile and model intensity belonging to start parameters of a least-squares-fit to the diffraction intensity of whole bacteria. $2^{n-1} = 16$ sign combinations for the moduli of the Fourier coefficients are shown. Each single presentations shows the electrondensity profile of three half periods with the distance statistics of the membrane distance above the point of contact of the half periods. The sign sequence gives the signs of the 1st to 5th Fourier coefficient. The diagram in the lower part shows the agreement between model intensity and experimental intensity for each start parameter set. The contributions of the model intensity between 0 and the 1st diffraction order are due to the correction functions for the differences between the electrondensity at the points of contact of the periods and the mean electrondensity of the stack. It can be seen that the peak heights are already fitted fairly well but that it will be difficult to describe the continuous background by means of the used model

considerably longer stacks. To give a better survey on the influences of the structure parameters onto the model intensity, Fig. 11 shows the electrondensity profiles and the corresponding model intensities for one set of start parameters. The corresponding experimental intensity, in this case measured on whole bacteria is also shown. All of the 16 single presentations show sign combinations

for the five Fourier coefficients necessary for the half period representation. As the model does not distinguish between solutions which only differ by reflection at the abscissa, the number of the possible sign combinations reduces from $2^5 = 32$ to $2^4 = 16$. The modulus of the Fourier coefficients was calculated by means of the area below the five diffraction orders. The 0th coefficient was set to 0, since an estimation was not possible. Further Fourier coefficients were not necessary, because in no case could more than five diffraction orders be detected. Stack extension and distance statistic parameters were estimated as described in "Material and methods". There was a mean stack extension of 4.6 periods. In accordance with the electronmicroscopic results (Fig. 6) one distance statistic was set very narrow. The broadening of the diffraction spots in this case is only caused by the intravesicular distance statistics. As mentioned before, membrane undulations were not taken into account. An examination of the 16 electrondensity profiles reveals that there are four groups each with four phases, possessing similar profiles. The groups are:

1) 1, 6, 11, 16,
2) 2, 5, 12, 15,
3) 3, 8, 9, 14,
4) 4, 7, 10, 13.

Two profiles each differ only by reflection at the abscissa and by displacement along the abscissa by a half period length, as for example 1 and 6, and 11 and 16 in the first group, however, the narrow and broad distance statistics are commuted. The commutation becomes evident in differences of the model intensity. Each model electrondensity in the 16 presentations shows three half periods. The left of the two contact points between the half periods must be assigned to the cytoplasmic side, the right contact point lies in the thylacoid lumen. This is due to the way in which the model considers the distribution of stack lengths, and it must be taken into consideration if one attempts to interpret the profiles. The similarity of the first two and the last two profiles in each group is due to the relative insignificance of a sign change of the first Fourier coefficient, because the modulus is small compared with the others. Therefore, only eight really different types of possible solutions exist. Between 0 and the first diffraction order of the intensity the influence of the interspace correction function becomes evident. If the electrondensities of one or both intermembranous spaces differ strongly from the mean electrondensity (in the above case = 0, beause the 0th Fourier coefficient is 0), there are considerable contributions in the area near the primary beam. One can see, however, that inspite of this, it is not possible to fit the very high continous scattering in this area even with the modified model. Similar problems appeared with intensities of crude thylacoid specimens. Satisfactory fits were only possible after introducing additional functions for the continuous intensity into the model. Because of the arbitrary shape of these functions a unique determination of the profile was not possible. Satisfactory and unique fits, without additional functions for the continuous intensity, were only achieved with purified thylacoids. As the influence of the first diffraction order was negligible, only 8 phase sets were started for fitting. After the end of the fit (stable ϕ-values) only 4

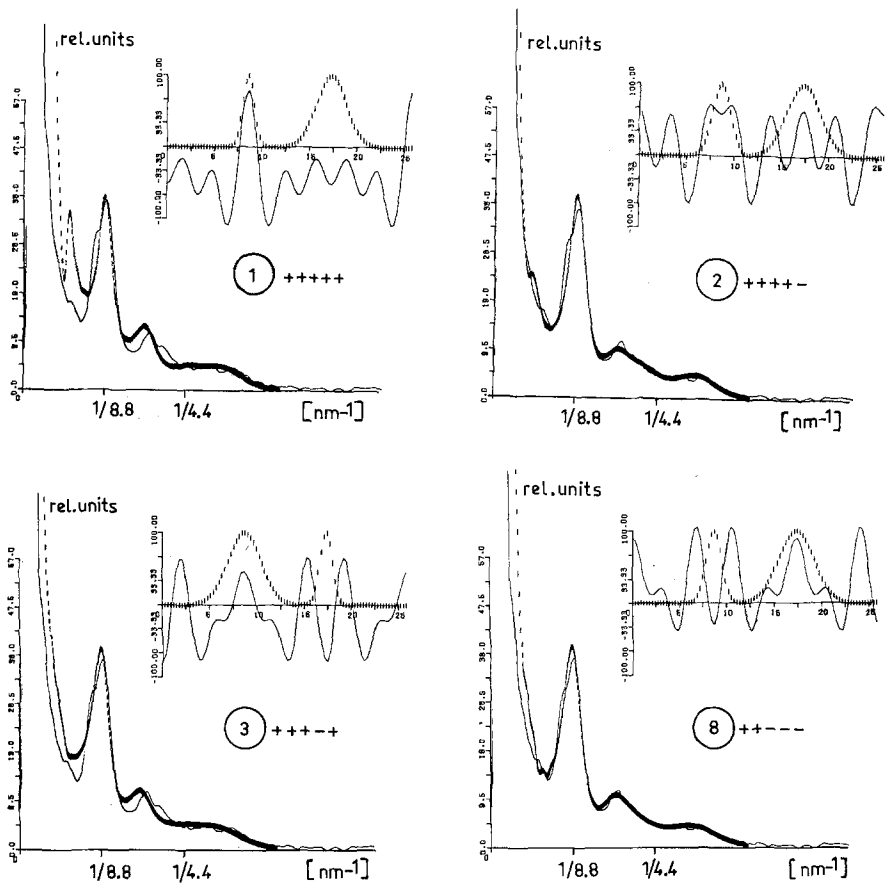

Fig. 12. Four phases, which did not alter the sign combination of the Fourier coefficients during the fit. The standard deviations of the distance statistics drawn above the points of contact of three half periods are: Phase 1: 0.62 nm, and 1.56 nm, phase 2: 0.95 nm, and 1.76 nm, phase 3: 0.66 nm, and 1.76 nm, and phase 8: 0.86 nm, and 2 nm. The smoothed experimental intensity is represented by the continuous line, the model intensity is plotted by the vertical bars. The fits are of different qualities. Phase 1 and 3 show bad agreement as to the experimental intensity, this means that they cannot be taken for solutions. Phase 2 and 8 are in good agreement with the experimental intensity. However, the better fitting in the region near the primary beam favours phase 2 as best solution. The Bragg-period is 17.6 nm

phase sets remained, the others had changed into already existing phase sets. Figure 12 shows the profiles of the remaining phase sets and their model intensities.

Discussion

Comparison: X-ray Diffraction and Electronmicroscopy

The evaluation of the electronmicrographs allowed an independent determination of statistical parameters which describe the behaviour of the membrane

distances and membrane undulations, whereas a resolution of these two statistical effects from X-ray diffraction patterns alone is very difficult. As the electronmicroscopic data provided evidence that the undulation influence can be neglected the model was limited to distance statistics. A comparison between electronmicroscopic and X-ray results shows that there is a good conformity of the overall periodicity. Moreover, both methods show different distance statistics and different mean membrane distances for the inter- and the intrathylacoid space. In the case of the suggested profile, which we believe to be the solution, both methods agree that the broader distance statistic belongs to the larger membrane distance. Not as good an agreement was achieved in the width of the two distance statistics. The electronmicroscopic evaluation gave considerable broader separation statistics than the X-ray diffraction patterns. This may be due to the slightly inadequate model assumption of lattice distortions of the second kind, and to influences by freezing in the electronmicroscopic specimens.

Electrondensity Profile Determination

The evaluation of the diffraction intensities for the determination of the electrondensity profile has shown that a unique determination of the profile is difficult even if the information lying between diffraction maxima is used. It is significant, whether and how the oriented continuous scattering was removed. Looking at phase 3 and 5 in Fig. 11 one can see that diminution of the continuous scattering, in a way which lowers the minima between the 2nd and 3rd diffraction to 0, but does not remove the intensity between the 4th and 5th order, definitely will favour phase 5. However, if the correction is chosen in the reverse way, phase 3 is favoured. For this reason we tried to integrate the oriented part of the continuous diffraction intensity into the model. As a satisfying description of the scattering intensity was only achieved for density-gradient-purified thylacoids, it must be assumed that the diffraction intensity of whole bacteria and thylacoid preparations contains substantial contributions of cell walls, cell membranes and soluble particles, which also align due to the platelet shape of the specimen. Besides the elimination of arbitrariness in determining the oriented continuous scattering, the modified model yielded a smaller number of possible solutions. Whereas evaluations where the oriented continuous background was eliminated by manual correction or by fitting additional functions, often yielded several phase sets with comparable fit quality, the modified procedure brought only one set of phases whose ϕ-value was better than that of the few remaining phase sets after the fit. There is only one further phase set which cannot be eliminated with absolute certainty as a possible solution, if only the criterion of the ϕ-value is applied. But there are further criteria which must be satisfied by the correct solution. These criteria are:

(4a) As the lipid content of viridis thylacoids is at least 30% as was shown above, there must be an area in the profile representing the carbon hydrate region of the lipids. This carbon hydrate area must have significantly less electrondensity than the part containing the lipid headgroups. As can be verified by Traube's volumes

[33] the mean electrondensity of the carbon hydrate groups lies between 160 and 280 e/nm^3; the mean electrondensity of polar headgroups is about 450 e/nm^3.
(4b) If one assumes that such minima of the electrondensity profile characterize the center of the membranes, the distances of the minima between the adjacent membranes of neighboured thylacoids must be less than the distance between the minima of membranes belonging to the same thylacoid, as shown in electronmicrographs.
(4c) The behaviour of the distance statistics must be consistent with the electronmicroscopic results, i.e., the standard deviation of the interthylacoid distances must be less than the standard deviation of the intrathylacoid distances.
(4d) For short stacks, as illustrated in "Material and methods" the differences between the mean electrondensities of the scattering region and the surrounding medium must be taken into consideration. This difference is described by the 0th Fourier coefficient of the half period Fourier-series in the modified model. The 0th Fourier coefficient lifts or lowers the profile until the abscissa has the level of the surrounding medium. If one takes Tris buffer for the surrounding medium, dried down to 1/5 of its initial volume, and calculates it electrondensity via the atomic volumes given by Traube, one gets a value of about 330 e/nm^3. The mean electrondensity of the thylacoid membrane containing 50% protein and 30% lipid is about 400 e/nm^3. This shows that the sign of the 0th Fourier coefficient must be positive. The remaining 20% of mass consisting of e.g., pigments and other lipids than phospholipids were not taken into consideration but it seems unlikely that they can markedly change the mean electrondensity.
(4e) The difference between the mean electrondensity of the membrane and the mean electrondensity of the surrounding medium (70 e/nm^3) may be used for an absolute calibration of the profile, because this difference corresponds with the height of the profile which is given by the 0th Fourier coefficient. As the 0th Fourier coefficient of the remaining phases varies considerably in relation to the peak heights, an absolute calibration may be regarded as a criterion as to whether the phase is a possible solution or not. For example, a calibration which leads to negative or to unreasonably high electrondensities, excludes such a profile as a solution.

The only electrondensity profile which satisfies the criteria *(4a–e)* is that of phase 2 in Fig. 12. This confirms that phase 2 gives the solution profile. Figure 13 shows the solution profile with an absolute calibration which was performed according to criterion *(4e)*. As a crude approximation we assume that the membrane lipids, which are at least 30% of the membrane dry weight, contribute to the electrondensity with the profile of a symmetric bilayer. If one substracts an adequate bilayer share from the calculated profile, one gets the electrondensity profile of the remaining membrane components. In our case we subtracted a profile as given in [34]. Due to the high content of protein, the difference will mainly represent the protein electrondensity distribution. If the electrondensity within the proteins is assumed to be constant, the difference curve is a measure for the volume distribution of the proteins in the membrane. From electronmicroscopic studies and also from X-ray diffraction experiments

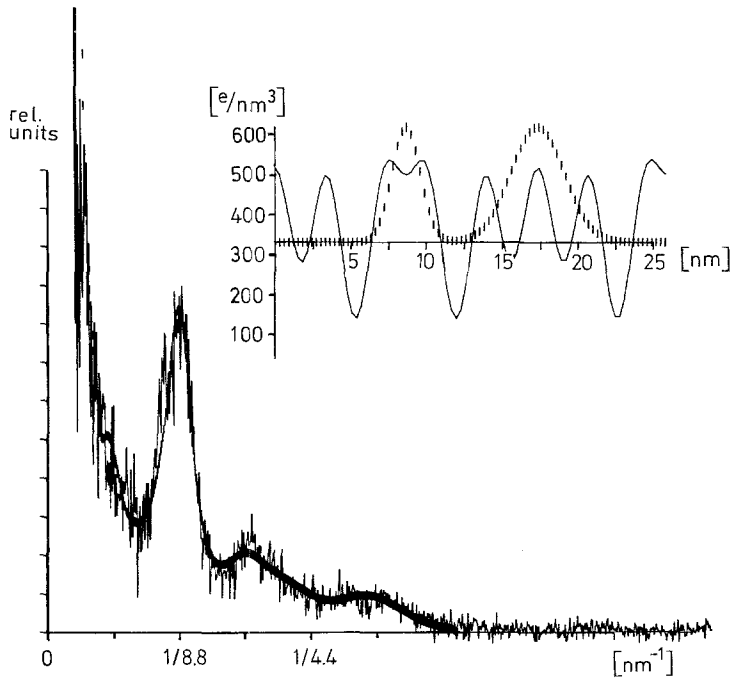

Fig. 13. Solution profile with an absolute calibration of the electrondensity scale. For this purpose the modulus of the 0th Fourier coefficient of the model electrondensity representation was equalized with the difference between the mean electrondensity of the stack and the mean electrondensity of the surrounding medium. In the lower part a comparison of the model intensity with the unsmoothed experimental intensity is given

we know, that there is a dense package and sometimes periodic arrangement of identical particles in the membrane plane as shown in Fig. 14. These particles represent the greatest share of the membrane volume. Therefore, the difference curve may also be looked at as the protein volume distribution in one unit cell of the membrane-crystal. Figure 15 shows therefore the difference curve as a volume distribution of the proteins in such a unit cell. This volume distribution has nearly equal protein shares for the both surface regions of the membrane and only a small amount of membrane-spanning components. This representation can only be regarded as a crude approximation since a systematic dependence of the protein electrondensity from the position on the stacking axis, due to varying hydrophobicity, may exist [35]. Such a dependence would level the marked fluctuations in the volume distribution. Also, there may be considerable deviations from the symmetric arrangement of the membrane lipids.

The distinct, high electrondensity peak in the center of the lumen might be caused by soluble lumen components, which are concentrated during the dehydration in the humidity chamber. An explanation for the distinct lumen peak is given in Fig. 16. It shows the projection of a dense package of homogenous spheres, which are aligned in the thylacoid lumen phase because of contact with membranous proteins. Another error in the electrondensity height

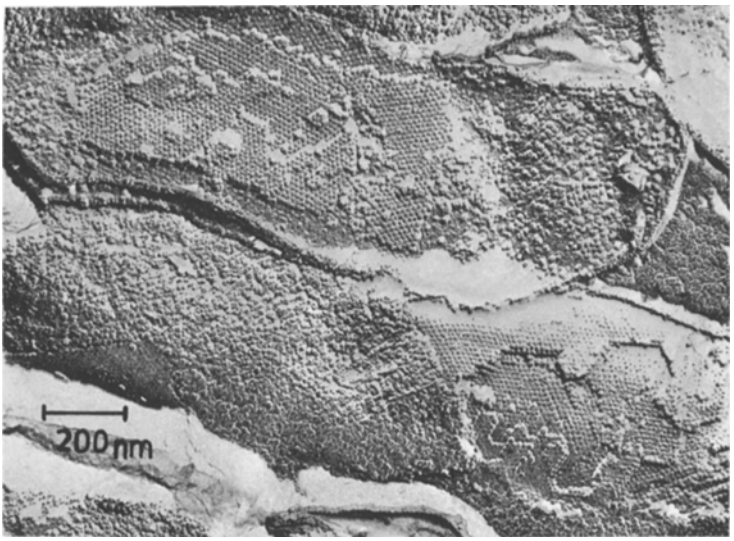

Fig. 14. Electronmicrograph of freeze fractured whole cells of Rhodopseudomonas viridis. The fracture plane reveals large areas with hexagonally arranged particles. The particle distance is about 13 nm

at the points of contact of the half periods may be caused by remains of oriented scatterers, whose intensity is falsely attributed to the stack intensity. This effect is caused by the property of the model, which tends to describe the underlying continuous intensity not only by means of the 0th Fourier coefficient but also by increasing the electrondensity difference between the density at the points of contact of the half periods and the mean density of the surrounding medium.

Unfortunately the electron density profile of the thylacoid membrane does not give information about the planar distribution of membrane components in a unit cell. The protein distribution shown in Fig. 15 is therefore an attempt to combine structural necessities, arising from functional experiments, with our protein volume evaluation. In this way the distribution in Fig. 15 agrees with the demand for a membrane spanning reaction center protein and an arrangement of most of the necessary components near the membrane surfaces as reported by Dutton and Prince [36].

Recent structural information about the in-plane structure of Rp. viridis thylacoids as stated by Miller [37] and Wehrli et al. [38] may also be supplemented by our evaluations. In [37] as well as in [38] a central particle in the unit cell is presumed, surrounded by membrane components in a way which yields sixfold symmetry of the unit cell at least on one side of the membrane. Our electron density profile suggests that, if the center contains the membrane spanning reaction center protein, the surrounding particles are independently arranged on both sides of the membrane without protein connection between them in the inner region of the membrane. The assumption of a different shape

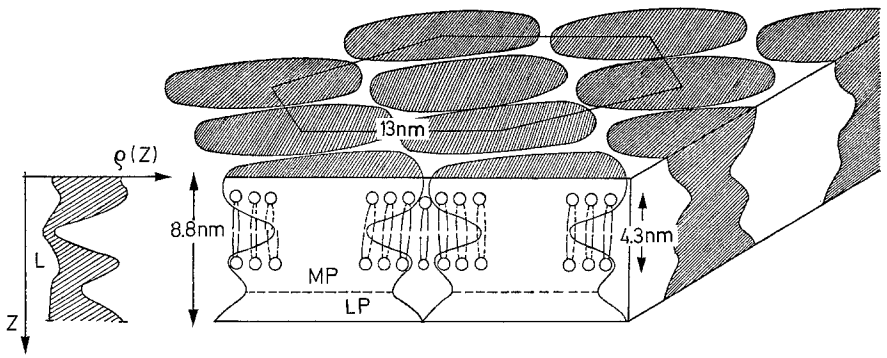

Fig. 15. A suggestion for the protein volume distribution in one unit cell of the planar lattice of Rhodopseudomonas viridis thylacoids. The left side shows the electron density profile $\varrho(z)$ with the lipid share of the membrane (L). The hatched area represents the difference, which is supposed to be mainly caused by protein contributions. The right side presents this area as protein volume of hexagonally arranged lattice cells. Possible lipid domains are shown by the lipid signs.The planar distribution of membrane components in the unit cell could not be described, because the electron density profile gives no information about it. The region occupied by luminal proteins is marked by LP, membrane protruding particles are characterized by MP. Some approximations had to be made: The lipid arrangement was assumed to be symmetrical, the contributions of non-lipid and non-protein components were neglected, and no systematic dependence of the protein electron density on the position along the stacking axis was taken into account

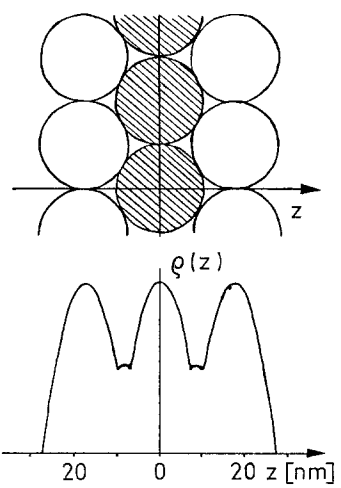

Fig. 16. Attempt to explain the distinct thylacoid lumen profile, by a projection of three rows of homogenous spheres onto the z-axis. The inner hatched row represents globular proteins in the lumen. The outer rows represent membrane protruding particles. All spheres must have a radius of about 1.0 nm to give a profile like that of the thylacoid lumen and its surrounding region as presented in Fig. 13

of the unit cell on both sides of the membrane is supported by observations made by Miller [37] as well as observations in electronmicrographs of our own laboratory.

Acknowledgements. We wish to thank C. Aehnelt, D. Deil, S. El-Deeb, J. Funk, G. Heppeler, W. Herbst, H. Oertwig, D. Walter, and E. Waidele for fruitful help and advice. Especially we want to thank W. Welte who contributed many ideas in our discussions during the investigations. All Computer calculations were done at the "Rechenzentrum der Universität Freiburg".

References

1. Takacs BJ, Holt SC (1971) Thiocapsa floridana, a cytological, physical and chemical characterisation. Biochim Biophys Acta 233: 258–277
2. Ota F, Fukui K, Morita J, Yoshida N, Kashiyama T (1973) Ultrastructure of Rhodospirillum rubrum after freeze-etching. Jpn J Microbiol 17: 527–529
3. Oelze J, Golecki JR (1975) Properties of reaction center depleted membranes of Rhodospirillum rubrum. Arch Microbiol 102: 59–64
4. Golecki JR, Oelze J (1975) Quantitative determination of cytoplasmic membrane invaginations in phototrophically growing Rhodospirillum rubrum. A freeze-etch study. J Gen Microbiol 88: 253–258
5. Lommen MAJ, Takemoto J (1978) Comparison, by freeze-fracture electron microscopy, of chromatophores, spheroplast-derived membrane vesicles, and whole cells of Rhodopseudomonas spheroides. J Bacteriol 136: 730–741
6. Golecki JR, Wakim B, Oelze J (1979) Differences in the architecture of the cytoplasmic membrane of phototrophically and chemotrophically grown representatives of the phototrophic bacteria. III Int. Symposium of Photosynthetic Procaryotes, Oxford (Abstract)
7. Zingsheim HP, Plattner H (1976) In: Korn ED (ed) Electron microscopic methods in membrane biology, vol 7. Academic Press, London, pp 56–90
8. Böhler S (1979) In: Rash JE, Hudson CS (eds) Freeze fracture: methods, artifacts and interpretations. Raven Press, New York
9. Ueki T, Kataoka M, Mitsui T (1976) Structural order in chromatophore membranes of Rhodospirillum rubrum. Nature 262: 809–810
10. Pape EH, Menke W, Weick D, Hosemann R (1974) Small angle X-ray scattering of the thylacoid membranes of rhodopseudomonas spheroides in aqueous suspensions. Biophys J 14: 221–232
11. Weick D (1974) Note on the theory of X-ray diffraction by spherical shell structures. Biophys J 14: 233–235
12. Kreutz W (1970) X-ray structure research on the photosynthetic membrane. Adv Bot Res 3: 53
13. Kreutz W (1964) Strukturuntersuchungen an Plastiden. Z Naturforsch 19: 441–446
14. Kreutz W (1964) In: Goodwin TW (ed) The structure of the lamellar system of chloroplasts, vol 1. Academic Press, London New York, pp 83–88
15. Sadler DM, Lefort-Tran M, Pouphile M (1973) Structure of photosynthetic membranes of euglena using X-ray diffraction. Biochim Biophys Acta 298: 620–629
16. Welte W, Kreutz W (1979) A general theory for the evaluation of X-ray diagrams of biomembranes and other lamellar systems. Adv Polymer Sci 30: 163–225
17. Drews G (1965) Isolierung schwefelfreier Purpurbakterien. Bakteriol Paras Infektionskr Hyg Abt Orig (Suppl) 1: 170–178
18. Horio T, Nishikawa K, Katsumata M, Yamashita J (1965) Possible partial reactions of the photophosphorylation process in chromatophores from Rhodospirillum rubrum. Biochim Biophys Acta 94: 371–382
19. Lowry OH, Rosebrough NJ, Farr AL, Randall RJ (1951) Protein measurement with the folin phenol reagent. J Biol Chem 193: 265–275
20. Bartlett GR (1959) Phosphorus assay in column chromatography. J Biol Chem 234: 466–468
21. Müller-Klieser W, Kreutz W (1976) On the cross-section structure of the mitochondrial cristae-membrane as revealed by X-ray diffraction. Z Naturforsch 310: 612–621
22. Kiessig HK (1942) Röntgenuntersuchung großer Netzebenenabstände und Untersuchung strömender Lösungen. Kolloid-Z 98: 213–221
23. Kratky O (1954) Neues Verfahren zur Herstellung von blendenstreuungsfreien Röntgen-Kleinwinkelaufnahmen. Z Elektrochem 58: 49–53
24. Broll N, Henne M, Kreutz W (1979) Eigenschaften und Anwendungsmöglichkeiten eines ortsempfindlichen Proportionalzählrohrs. Siemens Analysentechnische Mitteilung Nr. 271
25. Bevington PR (1969) Data reduction and error analysis for the physical sciences. McGraw-Hill Book Company, Toronto, New York

26. Frei M (1979) Anwendung eines neuen Auswerteverfahrens zur Röntgenstrukturanalyse von menschlichen Erythrozytenghosts unter besonderer Berücksichtigung des Membranzwischenraums und der Verwellungen der Membranoberflächen. Diplomarbeit, Inst. für Biophysik und Strahlenbiologie der Universität Freiburg im Breisgau, FRG
27. Hosemann R, Bagchi SN (1962) Direct analysis of diffraction by matter. North Holland, Amsterdam
28. Vainshtein BK (1966) Diffraction of X-ray by chain molecules. Elsevier Publishing, Amsterdam London New York
29. Marquardt DW (1963) An algorithm for least-squares estimation of nonlinear parameters. J Soc Ind Appl Math 2: 431–441
30. Papoulis A (1962) The fourierintegral and its applications. McGraw-Hill, Toronto New York
31. Schneider MJT, Schneider AS (1972) Water in biological membranes: adsorption isotherms and circular dichroism as a function of hydration. J Membr Biol 9: 127–140
32. Drews G (1968) Nachweis der Zucker in den Thylakoiden von Rhodospirillum rubrum und Rhodospseudomonas viridis. Z Naturforsch 23: 671–675
33. Traube J (1899) Über den Raum der Atome. Samm Chem Chem-Techn Vorträge 4: 1–78
34. Levine YK, Wilkins MHF (1971) Structure of oriented lipid bilayers. Nature [New Biol] 230: 69–72
35. Blaurock AE (1972) Structure of the retinal membrane containing the visual pigments. Adv Exp Med Biol 24: 53–63
36. Dutton PL, Prince RC (1978) In: Clayton RK, Sistrom WR (ed) Reaction-center-driven cytochrome interactions in electron and proton translocation and energy coupling. Plenum Press, New York London
37. Miller KR (1979) Structure of a bacterial photosynthetic membrane. Proc Natl Acad Sci USA 76: 6415–6419
38. Wehrli E, Kübler O, Koller T (1979) The architecture of the photosynthetic membrane of Rhodopseudomonas viridis. Experientia 35: 984

Received May 20, 1980/Accepted August 15, 1980